HHS Public Access

Author manuscript

Biomaterials. Author manuscript; available in PMC 2018 November 24.

Published in final edited form as:

Biomaterials. 2017 August ; 135: 42–52. doi:10.1016/j.biomaterials.2017.04.045.

Multimodal assessment of SERS nanoparticle biodistribution post ingestion reveals new potential for clinical translation of Raman imaging

Jos L. Campbell[a,b,c,+], **Elliott D. SoRelle**[a,d,e,+], **Ohad Ilovich**[a,c,f], **Orly Liba**[a,f,g], **Michelle L. James**[a,c], **Zhen Qiu**[a,c,h], **Valerie Perez**[a,c,i], **Carmel T. Chan**[a,c], **Adam de la Zerda**[a,d,e], and **Cristina Zavaleta**[a,c]

[a]Molecular Imaging Program at Stanford University, 318 Campus Dr. Stanford, CA 94305, United States

[b]RMIT University, Melbourne, Australia, 124 Latrobe St Melbourne, Victoria 3000, Australia

[c]Department of Radiology, Stanford University, 1201 Welch Rd. Stanford, CA 94305, United States

[d]Biophysics Program, Stanford University, 291 Campus Dr. Stanford, CA 94305, United States

[e]Department of Structural Biology, Stanford University 299 Campus Dr. Stanford, CA 94305, United States

[f]inviCRO, LLC, Imaging Services and Software, 27 Drydock Ave. Boston, MA 02210, United States

[g]Department of Electrical Engineering, Stanford University, 350 Serra Mall Stanford, CA 94305, United States

[h]Department of Pediatrics, 300 Pasteur Dr. H310 Stanford, CA 94305, United States

[i]Department of Chemical Engineering, Stanford University 443 Via Ortega Stanford, CA 94305, United States

Abstract

Despite extensive research and development, new nano-based diagnostic contrast agents have faced major barriers in gaining regulatory approval due to their potential systemic toxicity and prolonged retention in vital organs. Here we use five independent biodistribution techniques to demonstrate that oral ingestion of one such agent, gold-silica Raman nanoparticles, results in

Correspondence to: Cristina Zavaleta.

[+]Authors contributed equally

Author contributions

The manuscript was written through contributions of all authors. All authors have given approval to the final version of the manuscript.

Conflict of interest

The authors declare no competing financial interests

complete clearance with no systemic toxicity in living mice. The oral delivery mimics topical administration to the oral cavity and gastrointestinal (GI) tract as an alternative to intravenous injection. Biodistribution and clearance profiles of orally (OR) vs. intravenously (IV) administered Raman nanoparticles were assayed over the course of 48h. Mice given either an IV or oral dose of Raman nanoparticles radiolabeled with approximately 100μCi (3.7MBq) of ^{64}Cu were imaged with dynamic microPET immediately post nanoparticle administration. Static microPET images were also acquired at 2h, 5h, 24h and 48h. Mice were sacrificed post imaging and various analyses were performed on the excised organs to determine nanoparticle localization. The results from microPET imaging, gamma counting, Raman imaging, ICP-MS, and hyperspectral imaging of tissue sections all correlated to reveal no evidence of systemic distribution of Raman nanoparticles after oral administration and complete clearance from the GI tract within 24h. Paired with the unique signals and multiplexing potential of Raman nanoparticles, this approach holds great promise for realizing targeted imaging of tumors and dysplastic tissues within the oral cavity and GI-tract. Moreover, these results suggest a viable path for the first translation of high-sensitivity Raman contrast imaging into clinical practice.

Keywords

SERS Nanoparticles; Biodistribution; Raman Imaging; Systemic Toxicity; MicroPET

1. Introduction

Nanoparticles offer great potential as diagnostic contrast agents for cancer detection. Compared to their small molecule counterparts, nanoparticles can provide increased sensitivity via conjugation with multiple copies of targeting ligands. This greater ligand capacity can produce avidity effects that result in higher binding affinity to tumor cells.

This active targeting approach can also improve our understanding of various disease process at the cellular level. By targeting multiple cancer biomarkers, it is possible to produce molecular maps that convey important functional information about specific cancer types. For decades, physicians were limited to studying the structural details of lesions provided by traditional imaging techniques (i.e., x-ray, white light endoscopy). It wasn't until the first use of radiopharmaceutical contrast agents that an entirely new imaging field emerged. This field, called molecular imaging, has expanded to include the use of MRI, PET, SPECT ultrasound, photoacoustics, and even fluorescence imaging. Molecular imaging now offers physicians a new functional imaging tool that can facilitate earlier cancer detection and improved therapy response. As a result, many molecular imaging researchers have invested considerable effort into developing novel imaging strategies that include the use of nano-based contrast agents that can be used in conjunction with various and sometimes even multiple molecular imaging modalities [1–8].

Raman imaging with surface enhanced Raman scattering (SERS) nanoparticles has gained recent interest in the molecular imaging community due to its ultra-high detection sensitivity and unique multiplexing capabilities. This relatively new molecular imaging technique relies on the detection of light inelastically scattered by SERS nanoparticles (consisting of a gold

core, Raman active dye and silica shell) that are intended to act as tumor targeting beacons. The SERS nanoparticles used in this study are approximately 140 nm in diameter, can be easily conjugated with various tumor targeting ligands, and can be fabricated with various Raman-active dyes, each with its own distinct Raman signature to enable multiplexing. The local surface plasmon of the gold produces an enhancement in the local incident electromagnetic field near the conjugated Raman dye, thus increasing the Raman scattering cross-section of the dye by several orders of magnitude [9–11]. This effect provides the increased sensitivity required to detect down to pM concentrations of SERS particles in living mice [12]. This ultra-high sensitivity and the ability to multiplex up to 10 individual signals is made more attractive given the relatively inert gold core-silica shell composition [13, 14]. However these SERS nanoparticles, like many other nanoparticle constructs, have faced opposition for their use as diagnostic contrast agents due to concerns about their potential systemic toxicity and prolonged retention in the body.

In order to circumvent these toxicity issues, several reports have demonstrated the use of SERS nanoparticles for tumor targeting coupled with topical administration to epithelial targets [15–21]. Topical administration is highly advantageous when coupled with endoscopy, as it circumvents the low depth of penetration constraint often associated with optical imaging strategies and provides molecular information to clinicians during routine endoscopic examinations for dysplastic lesions. To this end, we have recently developed a clinical Raman endoscope that can be used in conjunction with existing clinical endoscopes as an accessory tool to provide functional imaging information [22–24]. Using SERS nanoparticles combined with an accessory Raman endoscopy device, clinicians can greatly enhance their ability to identify the location (and perhaps even the type) of a suspect region on the epithelial wall by coupling the molecular information from the tumor targeting nanoparticles with the structural information provided by conventional white light endoscopy.

In the current study, we extend the concept of low-toxicity topical administration to propose the use of SERS nanoparticles for oral and gastrointestinal imaging applications. Significant improvements in cancer detection are greatly needed for various epithelial cancers that occur within the length of the GI tract including oral, esophageal, gastric, small intestine, and colon cancers. It was recently reported that an estimated 236,000 people, within the US alone, will be diagnosed with one of these GI tract epithelial cancers this year [25]. Notably, GI cancers account for ~15% of all cancer related deaths in the United States each year[25], many of which can be prevented with earlier detection [26–28].

To determine whether the use of SERS particles for GI applications is feasible, we provide the first particle biodistribution and uptake data for orally-administered SERS nanoparticle contrast agents in live mice, and we compare the results from oral vs. more typical intravenous administration. We hypothesized that oral administration of SERS nanoparticles will prevent systemic exposure altogether and thus avoid any adverse toxicity effects or prolonged particle retention. As of this study, the distribution and clearance rates for this class of particle following oral delivery are not yet fully understood. Previous studies have demonstrated the ability of some nanoparticles to traffic into the blood after oral administration [29, 30] (albeit at exceptionally high dosages). Thus, it is critical to properly

examine and compare the biodistribution of our SERS nanoparticles after oral delivery of clinically-relevant dosages to determine whether they may be used in future clinical applications. We therefore conducted a rigorous biodistribution study using five independent techniques. In order to longitudinally track the particles without depth limitations, we first employed the use of microPET imaging. In such a study, it is critically important to conserve the surface chemistry of the nanoparticles to properly assess the true biodistribution and clearance kinetics of the SERS nanoparticles. For this reason, no additional linkers or molecules were added to the surface of the particles in order to attach the radiotracer for microPET imaging. Instead, ^{64}Cu was bound directly to the surface of the particles with a greater than 90% efficiency using already available thiolated surface chemistry. We further assessed SERS particle biodistribution by using dynamic microPET imaging, gamma counting of excised tissues, inductively coupled plasma mass spectrometry (ICP-MS) elemental analysis, and a new hyperspectral imaging technique that offers microscopic details of the gold-based SERS nanoparticle accumulation within histologically sectioned tissues. The results of all five methods demonstrate complete SERS particle clearance and no systemic uptake following oral administration. Consequently, these findings provide the strongest demonstration to date that SERS agents may gain regulatory approval for certain uses, thereby allowing potential clinical applications of Raman imaging in the future.

2. Methods

2.1 SERS nanoparticles

SERS nanoparticles were provided by Cabot Security Materials (formerly Oxonica Materials, Inc.) and comprised of a Au core of approximately 60-nm diameter coated with a monolayer of Raman-active organic molecule, Trans-1,2-Bis(4-pyridyl)-ethylene, and encapsulated with approximately 40-nm diameter thiolated silica shell, making the entire particle diameter on the order of ~140 nm (Supplementary Figure S1). The particular lot used in this study was the batch S440 that consists of a unique Raman active material and its associated spectrum, which can be seen in our previous work [14]. Toxicity studies on these particular nanoparticles have been previously published by our group [31, 32]. Additional particle characterization is provided in the supplementary information (Supplementary Figures S2–S5).

2.2 Chemical conjugation and radio-labeling of SERS nanoparticles

We tried several methods to radiolabel the thiolated silica coated nanoparticles including using various labeling techniques, incubation temperatures, buffers, pH levels, and blocking available binding sites to determine the best method to move forward with animal studies. We used a DOTA chelation technique; since there is high-affinity between Cu^{2+} ions and sulfur atoms, we assessed a non-linker based method with the thiolated nanoparticles as well [33, 34].

2.3 Conjugation with DOTA

For the DOTA conjugated group, the thiolated gold nanoparticles were functionalized with DOTA-maleimide to enable chelation of radioactive metal ions (in this case ^{64}Cu, $t_{1/2}$ = 12.7 h). Specifically: DOTA-maleimide was covalently conjugated to the thiolated surface of the

SERS nanoparticles via the addition of maleimide-DOTA (0.9 mg, 1.3 μmol) in 0.5 mL MES buffer (pH = 7.2) to SERS nanoparticles. Solution was stirred at room temperature overnight. Excess DOTA was separated from functionalized nanoparticles by three rounds of centrifugation (10,000 rpm, 4 min), and resuspension in MES buffer (pH = 7.2). DOTA-functionalized nanoparticles were finally suspended in deionized water (0.5 mL) for radiolabeling. An excess of n-ethyl maleimide was used to cap the excess thiol groups in one of the DOTA conjugated samples.

2.4 Protocol of SERS ^{64}Cu labeling

To determine the optimum radiolabeling conditions, the SERS nanoparticles were radiolabeled with ^{64}Cu by addition of $^{64}CuCl_2$ in either 0.01 N NaOAc (pH 5.0) buffer (for DOTA scenarios), MES (pH 5.5) buffer, or HEPES (pH 8.8) buffer followed by a 60 min incubation with SERS nanoparticles at either room temperature or 60°C with gentle shaking at 5 min. DOTA-chelated SERS nanoparticles were incubated at room temperature and centrifuged at 2,500 g for 3–5 min and washed with deionized water to remove non-bound free copper. The labeling yield and specific activity of each radiolabeling scenario is shown in Table 1. Rinsed SERS nanoparticle were resuspended in either deionized water, HEPES or MES buffer by sonicating and vortexing.

2.5 Animal experiments

Female 8 week old nude mice (Charles River) were used for all microPET and biodistribution studies. All procedures performed on the animals were approved by the University's Institutional Animal Care and Use Committee (APLAC #29179), and were within the guidelines of humane care of laboratory animals.

2.6 Animal injections

Mice were divided into two injection groups to evaluate differences in biodistribution between administering SERS nanoparticles intravenously (IV) versus orally (OR). Each group contained subgroups where mice were further separated to evaluate biodistribution at various time points post SERS nanoparticle administration. Three mice from each group were sacrificed at 2 h, 5 h, or 24 h to evaluate accumulation of SERS nanoparticles within specific organs of interest. We also included a group at 48 h that consisted of one mouse per administration route to confirm complete clearance of SERS nanoparticles from the GI tract after oral delivery. Mice in the IV group were given a 150 μL injection of approximately 100 μCi of ^{64}Cu-SERS nanoparticles (at a concentration of 0.8 nM) via the tail vein using a 26 gauge needle. Mice in the OR group also received a 150 μL administration of approximately 100 μCi of ^{64}Cu-SERS nanoparticles (at a concentration of 0.8 nM) using a disposable oral feeding needle with a standard oral gavage delivery technique.

2.7 MicroPET imaging

On the day of imaging, each mouse was anesthetized with 2.5–3% isoflurane delivered by 100% oxygen at 2 liters per minute through an isoflurane vaporizer. MicroPET imaging commenced immediately after injection of the ^{64}Cu-SERS nanoparticles. The mice were placed prone on the microPET bed and imaged with an Inveon MicroPET system

manufactured by Siemens. Dynamic microPET imaging commenced immediately post nanoparticle administration over the course of 2 hours (Supplementary Figure S6) and then 5 minute static images were acquired at 2h, 5h, 24h, and 48h. The images were then reconstructed using a three dimensional ordered subset expectation maximization (3D-OSEM) algorithm with a spatial resolution of 1.63 mm at the center of the field of view [35] and analyzed using Siemens Inveon Research Workplace software.

2.8 Biodistribution

After imaging, mice were then euthanized by cervical dislocation under deep isoflurane anesthesia. In each injection group (IV and OR) mice were sacrificed at 2h (n=3), 5h (n=3), 24h (n=3) and 48 h (n=1). Tissues were harvested, weighed and placed in scintillation vials for gamma counting. All harvested tissues were counted for 30 seconds in a Cobra II γ-counter (Packard/Perkin Elmer). An aliquot from the stock ^{64}Cu activity was also counted for data normalization. Results in Figure 3 are expressed as % injected dose per gram tissue (%ID/g).

2.9 Raman spectroscopic imaging in excised tissues

Tissues harvested at 2 h post nanoparticle administration (either IV or OR) were imaged using a Renishaw Raman microscope system. These images were acquired to verify the presence of SERS nanoparticles within specific organs of interest as indicated from microPET and gamma counting experiments. Organs from both IV and OR mice were separated into groups and imaged including organs responsible for systemic clearance of nanoparticles (i.e., liver, spleen, kidney etc.) and organs within the GI tract (i.e., stomach, small intestine, cecum, large intestine). A semiconductor diode near-infrared laser operating at λ=785 nm was used as the excitation source with a laser power of approximately 40 mW measured at the surface of the tissues. Raman images were obtained by using a Raman point mapping method. A computer-controlled x-y translation stage was used to raster-scan the tissues creating an intensity mapped image by measuring the Raman spectrum of each individual pixel in the area of interest with a 1 mm step size. Integration times of 1 seconds per step were acquired for each tissue Raman map. The objective lens used was 12x in a dimly-lit room.

2.10 Raman spectral analysis

The direct classical least squares (DCLS) method, also known as the linear un-mixing and K-matrix methods, was used in these experiments to perform analysis of Raman spectroscopy [36, 37]. DCLS finds the linear combination of spectra from the pure components within the sample that most closely matches the Raman spectrum of the sample. A pure component reference spectrum of the SERS nanoparticles used in this study was acquired for 1 s from a pure 5 μL sample aliquoted onto a piece of quartz under the microscope and used as the reference spectrum for the Raman analysis of the tissues harvested from the mice.

2.11 ICP-MS analysis

Organs of interest such as the liver, spleen, stomach, large intestine, and blood were further analyzed using ICP-MS. Before analysis the tissues were digested using a Mars Express microwave digester manufactured by CEM Inc. Organs were placed in Teflon microwave digestion tubes with 2 ml of hydrochloric acid and 5 ml of nitric acid. The tubes were evenly dispersed in the microwave digestion cylinder and set for 1600 W at 100% power for 25 min at 180 degrees C. The samples were then diluted and prepared for ICP-MS analysis. A standard curve was prepared using AuCl measured from 100 ppb down to 3.125 ppb (limit of detection). Samples were measured for the element gold (Au) on a Thermo Scientific* XSERIES 2 ICP-MS machine.

2.12 Hyperspectral microscopy imaging

All hyperspectral microscopy with adaptive detection (HSM-AD) was performed as described previously by SoRelle *et al* [38]. Briefly, mice treated either IV or orally with particles were euthanized at 2 or 24 hours, after which relevant tissues were resected and fixed in 10% formalin. Control tissues from uninjected mice were also collected and fixed. Fixed tissues were then embedded in paraffin, sectioned into 5 μm-thick slices, and mounted on microscope slides. Slides were de-paraffinized and imaged with a custom dark-field microscope with a hyperspectral camera (CytoViva, Auburn, AL). Acquired hyperspectral images were processed and analyzed using customized detection algorithms to identify particles in tissues by their unique scattering spectra. HSM-AD images depict tissue scattering intensity in grayscale and maps of particle accumulation (i.e., image pixels that display the unique particle spectrum) in green. Extensive details regarding this alternate biodistribution assessment method can be found in SoRelle *et al* [38].

2.13 Statistical analysis

The data collected from this study were analyzed for statistical differences using a 95% confidence interval ($p < 0.05$). A student's t-test was used to compare the data of the IV group to the data of the OR group. An equality of variances test was performed and revealed little variance between the IV and OR groups. Therefore, a one-tailed t-test assuming equal variances was performed to determine statistical significance because it was hypothesized that the OR group would have localized uptake in the large intestine and perhaps some leakage into the cecum with little to no uptake in any other organ, whereas the IV group would have higher uptake in all organs subjected to systemic delivery. The values herein are reported as mean ± standard error of mean (SEM). The data from each of the time points correlated well with each other, therefore, a Bonferroni correction was not indicated as it was too conservative, and there was little chance of getting a significant result from multiple t-testing.

3. Results

3.1 Radiolabeling optimization

The Raman nanoparticles evaluated in this study consist of a gold core, a Raman active layer adsorbed onto the gold core, and a thiolated silica shell totaling a diameter of approximately

140 nm (Supplementary Figure S1). The nanoparticle size was determined using dynamic light scattering (DLS) (Supplementary Figure S2), and their zeta potential was determined to be approximately −31.6 mV (Supplementary Figure S3). Further nanoparticle characterization and elemental analysis was determined using high resolution TEM, Energy-dispersive x-ray scattering (EDS), and Scanning Transmission Electron Microscopy (STEM) (Supplementary Figures S4–S5). We set up various radiolabeling experiments to evaluate which radiolabeling method would give us high labeling efficiencies while demonstrating good stability over time (minimal leaching effects after a 24 hour period). ^{64}Cu was chosen due to its sufficiently long half-life (12.7 hours), which lent itself well to 48 hour microPET biodistribution studies and its amicable binding chemistry.

Chelators such as DOTA are commonly used to attach metal-based radioisotopes to target surfaces or molecules [39–42]. However, the lower pH required to complete the DOTA conjugation can destabilize the colloidal SERS nanoparticles. Therefore, we assessed an alternative thiol based binding method that would minimize perturbation of the native thiolated nanoparticle surface chemistry. Since there is a high affinity between Cu2+ ions and sulfur atoms, the thiolated surface of the SERS nanoparticle is a perfect platform for radiolabeling with ^{64}Cu [33, 34]. We compared the effects of temperature, pH, and buffer composition to optimize the binding of ^{64}Cu to the sulfur atoms present on the SERS particles (Figure 1) [34, 43].

We observed the highest ^{64}Cu binding efficiency and retention over a 24 h period using a pH of 8.8, which is the native pH of the nanoparticles themselves (Figure 1). When we tried to use a DOTA chelation strategy the required pH of 5.5 disrupted the nanoparticles, causing them to stick to the walls of the tube and even precipitate out at times. As seen in Figure 1, we achieved a labeling efficiency as high as 96% with only 4% free ^{64}Cu leaching after EDTA addition and 24 hours incubation at room temperature in HEPES buffer at pH 8.8.

3.2 MicroPET imaging

After determining the most stable and efficient radiolabeling technique, we proceeded with administering the radiolabeled nanoparticles to follow their distribution throughout the body using microPET and gamma counting. Female nude mice were given either an IV or oral dose of SERS nanoparticles, at a concentration of 0.8 nM, labeled with approximately 100μCi (3.7 MBq) of ^{64}Cu in a 150 μL volume. Dynamic microPET imaging commenced immediately post nanoparticle administration, allowing us to track the uptake within the liver over the first 2 hours. The liver was a focal point for this experiment since it is the primary organ by which nanoparticles of this size are cleared from the blood and therefore serves as an indicator for systemic entry after nanoparticle administration.

Region of interest (ROI) analysis on the microPET images demonstrated rapid accumulation of SERS nanoparticles in the liver within the first five minutes post IV injection followed by continuous localization for the remainder of the 2 h dynamic imaging series (Supplementary Figure S6). In contrast, mice receiving an oral dose of SERS nanoparticles revealed no accumulation within the liver over the 2 hour dynamic scan, consistent with no systemic entry of the orally administered nanoparticles during this time period. Free ^{64}Cu doses were also administered both intravenously and orally in a separate group of mice to account for

any potential leaching of the radioactive agent from the nanoparticles. Static microPET images were also acquired at 2h, 5h, 24h, and 48h (Figure 2).

MicroPET images after oral administration reveal a consistent pattern of initial accumulation in the stomach at 2 hours before proceeding through the small intestine, cecum, and large intestine. By 24 hours the signal is barely detectable in mice that were orally dosed. Mice injected IV show a very different distribution of nanoparticles, with high initial uptake in the liver and spleen and retention of signal throughout the entire 48 hour imaging time course.

3.3 Gamma counting

After 2, 5, 24, or 48 hours, the mice from all groups (IV SERS, oral SERS, and free ^{64}Cu) were sacrificed and the organs were harvested for gamma counting to determine percent injected dose per gram (%ID/g) of nanoparticles within each tissue. Gamma counting revealed the majority of the nanoparticles were confined to the digestive system for mice receiving oral administration including stomach, small intestine, cecum and large intestine. By comparison, the IV injected mice displayed the most significant uptake in the liver and spleen, which persisted throughout the 48 hour period (Figure 3). By 24 hours post oral administration, the gamma counted organs revealed that most of the nanoparticles had been cleared via the rectum/feces. Additional biodistribution data from other organs can be found in Supplementary Figure S7 within the supplementary information.

Supplementary Figure S8 illustrates the difference in biodistribution between radiolabeled SERS nanoparticles and free ^{64}Cu after both oral and IV administration up to 24 hours. We see evidence of distinct biodistribution patterns between the data sets with IV administered materials being dominantly taken up and retained in the liver and spleen, while all orally administered materials tending to remain mostly confined to the organs of the intestinal tract, the stomach, small intestine, cecum and large intestine.

A point of interest was the larger variability observed between mice in the oral group (Figures 3, Supplementary Figure S8). This variability was particularly notable in the earlier time points (2 h and 5 h) post nanoparticle administration. As seen in Figure 3, this variability is localized to organs within the GI tract and is likely a result of the different digestion stages of the mice during nanoparticle administration. The mice were not fasted prior to nanoparticle administration and were likely on different eating cycles, which gave rise to this variability.

Notably, the only organ with significant signal post oral administration outside of the intestinal tract is the liver. This is likely due to some free ^{64}Cu that has leached from the SERS particles entering the bloodstream and being retained in the liver, as this is the primary excretion site for Cu ions in the bloodstream [40, 44, 45]. The observation that no significant signal is observed in the spleens of the orally dosed mice lends further credence to this explanation for the observed liver signal, especially considering the ratio of liver/spleen signal observed in the IV injected mice. However, in order to accurately determine the origin of this liver signal in orally dosed mice, additional analysis techniques are required. In this case we utilized *ex vivo* Raman imaging (Figure 4), ICP-MS (Figure 5), and a new hyperspectral imaging technique called HSM-AD (Figures 6,7), all of which indicated that

there was no presence of gold within the livers or spleens of mice that received oral doses of SERS particles.

3.4 Raman imaging

Organs were harvested from mice 2 hours post nanoparticle administration and mapped using our Raman imaging system to validate the microPET and biodistribution data at the same 2 hour time point. The Raman images reveal nanoparticle accumulation within the liver and the spleen of the IV injected mice, whereas the orally injected mice show no trace of nanoparticle accumulation in these organs **(**Figure 4). The mice given an oral dose of nanoparticles showed localization within the GI tract, particularly within the stomach and small intestine at the 2 hour time point. These Raman images reaffirm that the orally-administered nanoparticles are not detectable within organs associated with blood clearing at this time point, as would be expected if the SERS particles were entering the blood stream.

3.5 ICP-MS data

Since the nanoparticles largely consist of gold, we used ICP-MS to detect their presence within harvested tissue samples at various time points post nanoparticle administration. Due to the lack of endemic gold within the mice, ICP-MS was an ideal technique to determine the fate of the SERS nanoparticles of both administration routes. Whole organs harvested from mice at each time point were digested and analyzed for Au content with a detection threshold of ≈3 ppb. The ICP-MS data correlated well with the microPET and gamma counting analysis. Gold was localized to the liver and spleen of the mice injected intravenously (Figure 5). Whereas the mice injected orally showed initial accumulation in the stomach and large intestine, with no gold detected in either the liver or spleen throughout the 24 hour time period. Given that no gold traces are observed in the liver or spleen, this result supports the notion that the low but noticeable liver signal in orally dosed mice under gamma counting analysis was due to disassociated free ^{64}Cu that had become unbound from the SERS nanoparticles and made its way to the liver. At the 24 hour time point, no significant gold signal could be detected in any organ for the orally administered mice. This also supports the concept that these particles undergo complete clearance within approximately 24 hours.

3.6 Hyperspectral microscopy imaging

To confirm ICP and radioisotope biodistribution results with high sensitivity and the added benefit of histological detail, tissue samples from each experimental condition were analyzed using hyperspectral microscopy with adaptive detection (HSM-AD) [38]. HSM-AD was used to identify particles in histological sections with high specificity and single-particle sensitivity based on detection of their unique plasmonic resonance peak at 550 nm (Figure 6). As expected, tissues resected from control mice exhibited virtual absence of particle signal. By The images shown in Figure 6 are a subset of all analyzed images; a more complete and quantitative representation of the data is provided in Supplementary Figure S9 within the supplementary information. As a note, the hyperspectral images in Figure 6 visually convey the spatial distribution of particles in tissue, however the images alone do not directly correlate to quantitative uptake in each organ because they do not visually

represent signal intensity (this is the basis for the apparent, but not actual, greater uptake of particles in the spleen versus liver). Signal intensity is taken into account in Supplementary Figure S9, the results of which agree well with quantification from ICP-MS. Substantial particle presence was observed in liver and spleen tissue at 2 and 24 hours after IV injection as well as in sections of stomach and large intestine of mice 2 hours after oral administration. Notably, particles were not detected in the stomach or large intestine 24 hours after oral administration, indicative of complete clearance via excretion. While orally-administered particles were able to access the surface of the stomach and large intestine epithelium, it was observed that particles were absent from the tissue proper at both 2 and 24 hours. Moreover, no nanoparticles were identified in liver or spleen tissue after oral administration. These results provide strong evidence that orally-delivered particles do not translocate from the lumen into gastrointestinal tissues, nor do they leak into systemic circulation. This data corroborates both the ICP-MS and gamma counting results that no presence of the SERS nanoparticles is detectable outside of the intestinal system when orally administered.

High-magnification HSM-AD images reveal unique patterns of particle accumulation in tissues 2 hours following intravenous and oral administration. IV administered particles accumulate in high density within the Kupffer cells of the liver (Figure 7a) and in the splenic marginal zone found between blood-filtering red pulp and lymphocyte-containing white pulp follicles (Figure 7b). Stomach and large intestine sections (Figure 7c, 7d) exhibit substantial presence of particles within the space of the gastrointestinal lumen, however negligible particle signal was observed within columnar epithelial tissue itself. As noted previously, particle detection was negligible 24 hours after oral delivery in both the GI lumen and epithelium.

4. Discussion

This study set out to determine the fate of orally administered SERS nanoparticles so as to mimic the topical application of such materials to epithelial targets within the oral cavity or any region of the gastrointestinal tract. To accomplish this, five separate techniques were utilized to overcome the real world difficulty of accurately and quantitatively localizing the uptake and bio-distribution of these nanoparticles in a living animal model. On their own, each of these techniques has failings and difficulty with absolute certainty as to the real biodistribution, however together they produce a strong library of cross referenced data to discuss.

It is clear from each of the results in Figures 2–7 that the accumulation profile that occurs after IV administration is significantly different from particles given orally. IV injection leads to rapid uptake in the liver and spleen (Supplementary Figure S2) where the particles remain throughout the 48 hour time period. Considering that the primary organs responsible for clearing nanoparticles from the blood include both the liver and spleen, these results fit with expectations that particles of this size (~140 nm) would be rapidly cleared from the blood. This also means that any particles that breached the gut lumen after oral administration would quickly find themselves trapped in the liver or spleen, where the

accumulation would lead to a steady increase in detectable liver signal over time; however, this result was not observed.

A key point of interest is the value of the HSM-AD analysis, which not only provides highly sensitive and specific detection of gold within tissue sections but also reveals microscopically where within tissues the particles are being retained. As can be observed in Figure 7, HSM-AD confirms that, in the case of oral administration, the particles are contained within the GI lumen and that the lumen wall provides a sufficient barrier to retain the particles. Clear definition can be observed between the external and internal tissue regions (Figure 7c, 7d). SERS particles occupy the internal space of the gut and stick to the walls of the epithelium, but no significant signal can be observed outside of the luminal space. Liver and spleen sections of mice after IV administration clearly show sub organ localization specific to Kupffer cells in the liver and within the marginal zone of the spleen (Figure 7a, 7b). Perhaps the most compelling finding from HSM-AD analysis is that nanoparticles can access the gastrointestinal epithelium without undergoing non-specific accumulation. In theory, this would enable future high-specificity identification of nanoparticles targeted to specific epithelial biomarkers expressed in certain gastric, colorectal, and esophageal cancers. The application of targeted variants of the nanoparticles tested herein for cancer biomarker detection is one focus of our current and future research.

The other primary result observable in Figures 2–7 is that each tracking modality used (radio labeling, gold elemental analysis, Raman, and hyperspectral imaging) consistently demonstrate that SERS nanoparticles administered orally are cleared from the body within approximately 24 hours. This is an important factor when considering the translation of nanoparticle-based imaging strategies to a clinical setting. Reliable clearance significantly reduces concerns regarding toxicity or long term retention that complicate the risk assessment when developing nanoparticle-based clinical approaches to disease. There are several clinical diseases which could be investigated using this imaging approach since multiple tissue/organ sites occupy the length of the GI tract. As previously noted, these sites include the oral cavity, esophagus, stomach, small intestine, and large intestine. All of these regions can be easily targeted post-ingestion with these tumor targeting SERS nanoparticles and most are readily accessible for imaging using a fiber optic based Raman endoscopic probe [19, 22, 24].

SERS nanoparticles also have great potential to be used as tumor targeting contrast agents to guide surgery in real time. Oral cancer surgery suffers from poor tumor margin delineation which results in lengthy and repeat surgeries. Complete removal of the primary tumor is the most important prognostic factor, since patients with “positive” surgical margins have a statistically significant decrease in survival [46]. One of the biggest challenges faced by oncologic surgeons in the operating room is determining where the tumor they are resecting begins and ends. These tumor targeting SERS nanoparticles could be applied topically to the oral cavity in the form of a rinse and, when used with a handheld Raman imaging device [16, 17, 19, 22, 24], provide surgeons with a molecular imaging map that offers objective, actionable information in real-time to guide tumor resection and thereby improve patient outcomes.

Because these nanoparticles are made of gold they also have the potential to be used therapeutically, in conjunction with an external laser excitation source, for photothermal ablation of targeted cancer tissues. After continued research and further development, this theranostic technique has great potential to improve clinical patient care.

It is conceivable that other nanoparticles, particularly in this size range, may have similar distribution properties within the GI tract post ingestion and should be studied for both imaging and therapeutic potential. A number of nano-based chemotherapeutic drugs are currently being used clinically to help localize therapy and reduce systemic toxicity after IV injection [47, 48].

Consistent with the findings reported herein, oral administration of these nano-based chemotherapy drugs could offer a better alternative to treating cancers affecting the epithelial wall of the GI tract and further reduce systemic toxicity to the patient. Thus, further investigation of these clinically approved nano-based drugs should be conducted to study their distribution and therapeutic effect after oral dosing.

5. Conclusion

Our findings reveal that the SERS Raman nanoparticles evaluated in this study remain localized in the digestive system and do not enter the bloodstream after oral administration. Additionally, the results indicate that the orally administered nanoparticles leave the body within 24 hrs. Five independent techniques corroborate these statements of clearance time and biodistribution. The data suggests that there would be no significant systemic toxicity since the orally administered nanoparticles do not enter the bloodstream or accumulate in the primary organs (liver or spleen) responsible for filtering this size of nanoparticle after systemic entry. In addition to providing the first oral biodistribution data for Raman contrast agents, our findings have the potential to accelerate the regulatory process to promote a molecular imaging strategy that utilizes a topical administration of tumor targeting nanoparticles to the oral cavity or GI tract. Such regulatory approval is vital for realizing the clinical translation of tumor targeted nano-based contrast agents in conjunction with molecular imaging for the sensitive detection of various oral and GI cancers.

Supplementary Material

Refer to Web version on PubMed Central for supplementary material.

Acknowledgments

Funding Sources

This work was supported by the National Cancer Institute of the National Institutes of Health under Award Number K22 CA160834 as well as R21 CA184608. Jos Campbell was supported by the Victorian government of Australia in the form of a Victorian postdoctoral research fellowship. We would like to thank Roopa Dalal for her help with tissue sectioning and staining and Frezghi Habte and Tim Doyle for their help with microPET imaging and post-processing troubleshooting. We would also like to thank Ai Leen Koh for her help with acquiring TEM and EDS data.

Appendix A. Supplementary data

Supplementary data related to this article can be found separately.

Abbreviations

SERS	surface enhanced Raman scattering
MRI	magnetic resonance imaging
SPECT	single photon computed tomography
PET	position emission tomography
DCLS	direct classical least squares
HSM-AD	hyperspectral microscopy with adaptive detection
IV	intravenously
OR	orally
GI	gastrointestinal
^{64}Cu	Copper-64
%ID/g	percent injected dose per gram
ICP-MS	inductively coupled plasma mass spectrometry
3D OSEM	three dimensional ordered subset expectation maximization
ROI	region of interest
APLAC	administrative panel on laboratory animal care
SEM	standard error of mean
TEM	transmission electron microscopy
EDS	energy-dispersive x-ray scattering
STEM	scanning transmission electron microscopy

References

1. Atukorale PU, Covarrubias G, Bauer L, Karathanasis E. Vascular targeting of nanoparticles for molecular imaging of diseased endothelium. Advanced drug delivery reviews. 2016
2. Hill TK, Mohs AM. Image-guided tumor surgery: will there be a role for fluorescent nanoparticles? Wiley interdisciplinary reviews Nanomedicine and nanobiotechnology. 2016; 8:498–511. [PubMed: 26585556]
3. Kirschbaum K, Sonner JK, Zeller MW, Deumelandt K, Bode J, Sharma R, et al. In vivo nanoparticle imaging of innate immune cells can serve as a marker of disease severity in a model of multiple sclerosis. Proceedings of the National Academy of Sciences of the United States of America. 2016

4. Mehta A, Ghaghada K, Mukundan S Jr. Molecular Imaging of Brain Tumors Using Liposomal Contrast Agents and Nanoparticles. Magnetic resonance imaging clinics of North America. 2016; 24:751–63. [PubMed: 27742115]
5. Mi P, Wang F, Nishiyama N, Cabral H. Molecular Cancer Imaging with Polymeric Nanoassemblies: From Tumor Detection to Theranostics. Macromolecular bioscience. 2016
6. Mohs AM, Mancini MC, Provenzale JM, Saba CF, Cornell KK, Howerth EW, et al. An integrated widefield imaging and spectroscopy system for contrast-enhanced, image-guided resection of tumors. IEEE transactions on bio-medical engineering. 2015; 62:1416–24. [PubMed: 25585410]
7. Shen Z, Wu A, Chen X. Iron Oxide Nanoparticle Based Contrast Agents for Magnetic Resonance Imaging. Molecular pharmaceutics. 2016
8. Thakor AS, Jokerst JV, Ghanouni P, Campbell J, Mittra E, Gambhir SS. Clinically Approved Nanoparticle Imaging Agents. Journal of nuclear medicine: official publication, Society of Nuclear Medicine. 2016
9. Faulds K, Barbagallo RP, Keer JT, Smith WE, Graham D. SERRS as a more sensitive technique for the detection of labelled oligonucleotides compared to fluorescence. The Analyst. 2004; 129:567–8. [PubMed: 15213819]
10. Fleischmann M, Hendra PJ, McQuillan AJ. Raman Spectra of Pyridine Adsorbed at a Silver Electrode. Chem Phys Lett. 1974; 26:163–6.
11. Wang DS, Chew H, Kerker M. Enhanced Raman scattering at the surface (SERS) of a spherical particle. Applied optics. 1980; 19:2256–7. [PubMed: 20234398]
12. Keren S, Zavaleta C, Cheng Z, de la Zerda A, Gheysens O, Gambhir SS. Noninvasive molecular imaging of small living subjects using Raman spectroscopy. Proceedings of the National Academy of Sciences of the United States of America. 2008; 105:5844–9. [PubMed: 18378895]
13. Thakor AS, Jokerst J, Zavaleta C, Massoud TF, Gambhir SS. Gold nanoparticles: a revival in precious metal administration to patients. Nano letters. 2011; 11:4029–36. [PubMed: 21846107]
14. Zavaleta CL, Smith BR, Walton I, Doering W, Davis G, Shojaei B, et al. Multiplexed imaging of surface enhanced Raman scattering nanotags in living mice using noninvasive Raman spectroscopy. Proceedings of the National Academy of Sciences of the United States of America. 2009; 106:13511–6. [PubMed: 19666578]
15. Jokerst JV, Miao Z, Zavaleta C, Cheng Z, Gambhir SS. Affibody-functionalized gold-silica nanoparticles for Raman molecular imaging of the epidermal growth factor receptor. Small. 2011; 7:625–33. [PubMed: 21302357]
16. Wang Y, Kang S, Doerksen JD, Glaser AK, Liu JT. Surgical Guidance via Multiplexed Molecular Imaging of Fresh Tissues Labeled with SERS-Coded Nanoparticles. IEEE journal of selected topics in quantum electronics : a publication of the IEEE Lasers and Electro-optics Society. 2016; 22
17. Wang Y, Kang S, Khan A, Ruttner G, Leigh SY, Murray M, et al. Quantitative molecular phenotyping with topically applied SERS nanoparticles for intraoperative guidance of breast cancer lumpectomy. Scientific reports. 2016; 6:21242. [PubMed: 26878888]
18. Wang YW, Kang S, Khan A, Bao PQ, Liu JTC. In vivo multiplexed molecular imaging of esophageal cancer via spectral endoscopy of topically applied SERS nanoparticles. Biomedical Optics Express. 2015; 6:3714–23. [PubMed: 26504623]
19. Wang YW, Khan A, Leigh SY, Wang D, Chen Y, Meza D, et al. Comprehensive spectral endoscopy of topically applied SERS nanoparticles in the rat esophagus. Biomedical Optics Express. 2014; 5:2883–95. [PubMed: 25401005]
20. Wang YW, Khan A, Som M, Wang D, Chen Y, Leigh SY, et al. Rapid ratiometric biomarker detection with topically applied SERS nanoparticles. Technology. 2014; 2:118–32. [PubMed: 25045721]
21. WW Y, Doerksen JD, Kang S, Walsh D, Yang Q, Hong D, et al. Multiplexed Molecular Imaging of Fresh Tissue Surfaces Enabled by Convection-Enhanced Topical Staining with SERS-Coded Nanoparticles. Small. 2016
22. Garai E, Sensarn S, Zavaleta CL, Loewke NO, Rogalla S, Mandella MJ, et al. A real-time clinical endoscopic system for intraluminal, multiplexed imaging of surface-enhanced Raman scattering nanoparticles. PloS one. 2015; 10:e0123185. [PubMed: 25923788]

23. Garai E, Sensarn S, Zavaleta CL, Van de Sompel D, Loewke NO, Mandella MJ, et al. High-sensitivity, real-time, ratiometric imaging of surface-enhanced Raman scattering nanoparticles with a clinically translatable Raman endoscope device. Journal of biomedical optics. 2013; 18:096008. [PubMed: 24008818]
24. Zavaleta CL, Garai E, Liu JT, Sensarn S, Mandella MJ, Van de Sompel D, et al. A Raman-based endoscopic strategy for multiplexed molecular imaging. Proceedings of the National Academy of Sciences of the United States of America. 2013; 110:E2288–97. [PubMed: 23703909]
25. NIH. The Surveillance, Epidemiology, and End Results (SEER) Program. 2016
26. Vital Signs. Colorectal cancer screening, incidence, and mortality-United States, 2002–2010. MMWR Morb Mortal Wkly Rep. 2011:884–9. [PubMed: 21734636]
27. Winawer SJ, Zauber AG, Ho MN, O'Brien MJ, Gottlieb LS, Sternberg SS, et al. Prevention of colorectal cancer by colonoscopic polypectomy. The National Polyp Study Workgroup. The New England journal of medicine. 1993; 329:1977–81. [PubMed: 8247072]
28. Zauber AG, Winawer SJ, O'Brien MJ, Lansdorp-Vogelaar I, van Ballegooijen M, Hankey BF, et al. Colonoscopic polypectomy and long-term prevention of colorectal-cancer deaths. The New England journal of medicine. 2012; 366:687–96. [PubMed: 22356322]
29. van der Zande M, Vandebriel RJ, Groot MJ, Kramer E, Herrera Rivera ZE, Rasmussen K, et al. Sub-chronic toxicity study in rats orally exposed to nanostructured silica. Particle and fibre toxicology. 2014; 11:8. [PubMed: 24507464]
30. van der Zande M, Vandebriel RJ, Van Doren E, Kramer E, Herrera Rivera Z, Serrano-Rojero CS, et al. Distribution, elimination, and toxicity of silver nanoparticles and silver ions in rats after 28-day oral exposure. ACS Nano. 2012; 6:7427–42. [PubMed: 22857815]
31. Thakor AS, Luong R, Paulmurugan R, Lin FI, Kempen P, Zavaleta C, et al. The fate and toxicity of Raman-active silica-gold nanoparticles in mice. Science translational medicine. 2011; 3:79ra33.
32. Thakor AS, Paulmurugan R, Kempen P, Zavaleta C, Sinclair R, Massoud TF, et al. Oxidative stress mediates the effects of Raman-active gold nanoparticles in human cells. Small. 2011; 7:126–36. [PubMed: 21104804]
33. Liu T, Shi S, Liang C, Shen S, Cheng L, Wang C, et al. Iron oxide decorated MoS2 nanosheets with double PEGylation for chelator-free radiolabeling and multimodal imaging guided photothermal therapy. ACS Nano. 2015; 9:950–60. [PubMed: 25562533]
34. Zhou M, Zhang R, Huang M, Lu W, Song S, Melancon MP, et al. A chelator-free multifunctional [64Cu]CuS nanoparticle platform for simultaneous micro-PET/CT imaging and photothermal ablation therapy. Journal of the American Chemical Society. 2010; 132:15351–8. [PubMed: 20942456]
35. Magota K, Kubo N, Kuge Y, Nishijima K, Zhao S, Tamaki N. Performance characterization of the Inveon preclinical small-animal PET/SPECT/CT system for multimodality imaging. European journal of nuclear medicine and molecular imaging. 2011; 38:742–52. [PubMed: 21153410]
36. Haaland DM, Easterling RG. Improved Sensitivity of Infrared Spectroscopy by the Application of Least Squares Methods. Appl Spec. 1980; 34:539–48.
37. Pelletier MJ. Quantitative Analysis Using Raman Spectroscopy. Appl Spect. 2003; 57:20A–42A.
38. SoRelle ED, Liba O, Campbell JL, Dalal R, Zavaleta CL, de la Zerda A. A hyperspectral method to assay the microphysiological fates of nanomaterials in histological samples. eLife. 2016; 5
39. Li M, Meares CF, Zhong GR, Miers L, Xiong CY, DeNardo SJ. Labeling monoclonal antibodies with 90yttrium- and 111indium-DOTA chelates: a simple and efficient method. Bioconjugate chemistry. 1994; 5:101–4. [PubMed: 8031871]
40. Schipper ML, Cheng Z, Lee SW, Bentolila LA, Iyer G, Rao J, et al. microPET-based biodistribution of quantum dots in living mice. Journal of nuclear medicine : official publication, Society of Nuclear Medicine. 2007; 48:1511–8.
41. Wu AM, Yazaki PJ, Tsai S, Nguyen K, Anderson AL, McCarthy DW, et al. High-resolution microPET imaging of carcinoembryonic antigen-positive xenografts by using a copper-64-labeled engineered antibody fragment. Proceedings of the National Academy of Sciences of the United States of America. 2000; 97:8495–500. [PubMed: 10880576]

42. Zavaleta CL, Hartman KB, Miao Z, James ML, Kempen P, Thakor AS, et al. Preclinical evaluation of Raman nanoparticle biodistribution for their potential use in clinical endoscopy imaging. Small. 2011; 7:2232–40. [PubMed: 21608124]

43. Shaffer TM, Wall MA, Harmsen S, Longo VA, Drain CM, Kircher MF, et al. Silica nanoparticles as substrates for chelator-free labeling of oxophilic radioisotopes. Nano letters. 2015; 15:864–8. [PubMed: 25559467]

44. Frellsen AF, Hansen AE, Jolck RI, Kempen P, Severin GW, Rasmussen PH, et al. A Mouse Positron Emission Tomography Study of the Biodistribution of Gold Nanoparticles with Different Surface Coatings Using Embedded Copper-64. ACS Nano. 2016

45. Jorgensen JT, Persson M, Madsen J, Kjaer A. High tumor uptake of (64)Cu: implications for molecular imaging of tumor characteristics with copper-based PET tracers. Nuclear medicine and biology. 2013; 40:345–50. [PubMed: 23394821]

46. Ravi SB, Annavajjula S. Surgical margins and its evaluation in oral cancer: a review. J Clin Diagn Res. 8:ZE01-5.

47. Mudshinge SR, Deore AB, Patil S, Bhalgat CM. Nanoparticles: Emerging carriers for drug delivery. Saudi pharmaceutical journal : SPJ : the official publication of the Saudi Pharmaceutical Society. 2011; 19:129–41. [PubMed: 23960751]

48. Thakor AS, Gambhir SS. Nanooncology: the future of cancer diagnosis and therapy. CA: a cancer journal for clinicians. 2013; 63:395–418. [PubMed: 24114523]

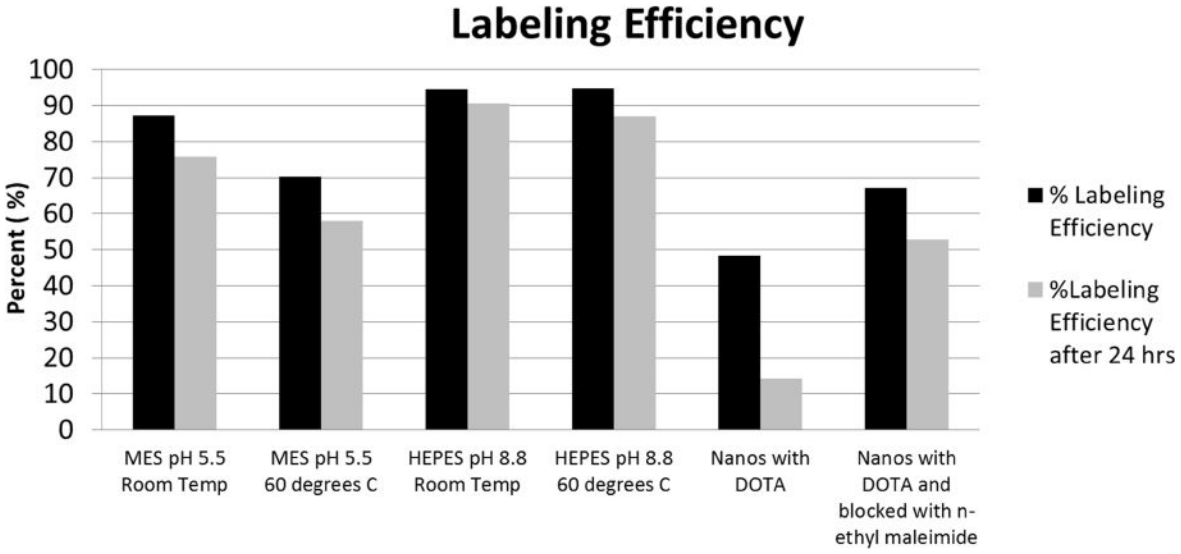

Figure 1.

Labeling efficiency of Cu to Raman nanoparticles using various labeling strategies, incubation temperatures, and pH buffers.

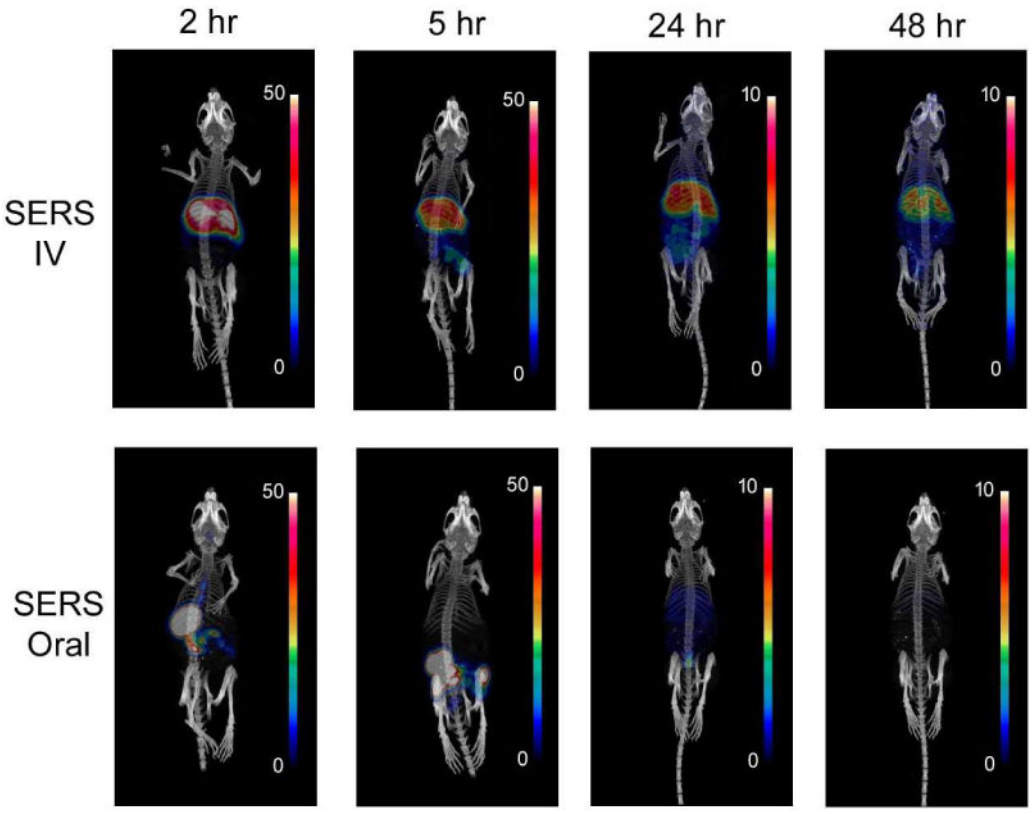

Figure 2.

Static microPET images at 2, 5, 24 and 48 hour time points post IV or oral administration of radiolabeled SERS nanoparticles. Scale bar indicates % injected dose per gram (%ID/g) of tissue.

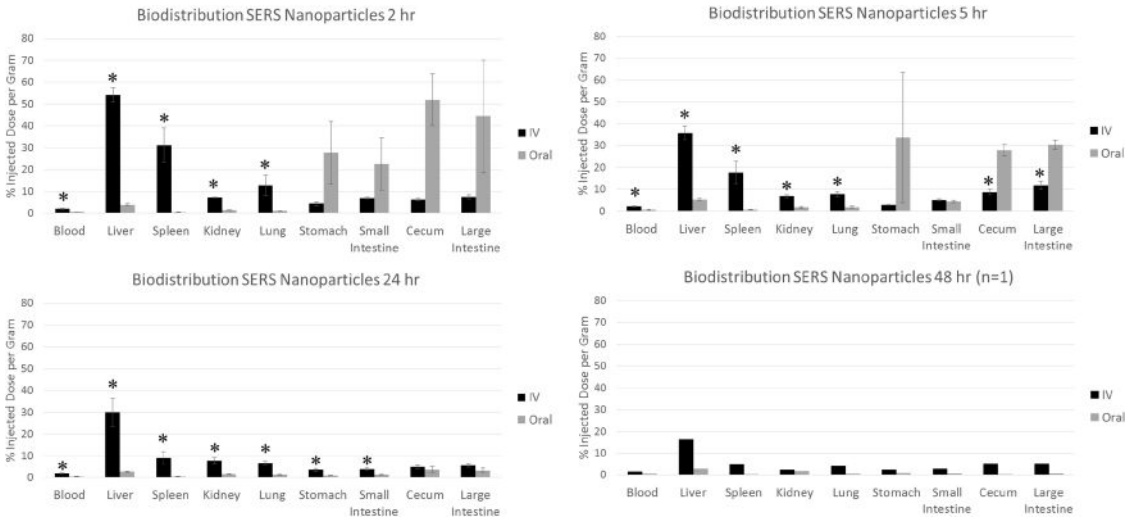

Figure 3.

Biodistribution of ^{64}Cu-labled Raman nanoparticles post IV vs oral administration. Gamma counting of individual organs revealed a significant difference in nanoparticle accumulation between IV and oral groups. Mice receiving IV injection of nanoparticles had significantly higher accumulation in most organs (*depicts $p < 0.03$), particularly those involved in the systemic clearance of nanoparticles (i.e., liver, spleen). Additional organs with considerably less uptake can be seen in Supplementary Figure S7 within supporting information. Error bars represent standard error of the mean.

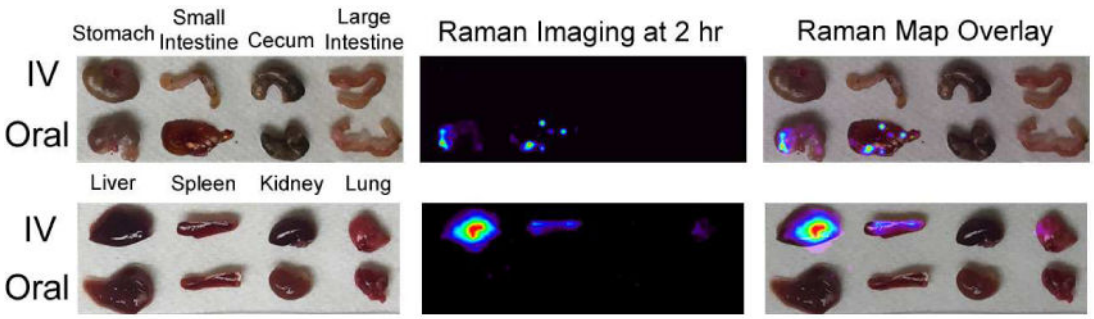

Figure 4.

Raman imaging confirms the localization of the Raman nanoparticles in the liver and spleen of the intravenously injected mice, whereas the orally injected mice show no sign of nanoparticles within the systemic organs imaged.

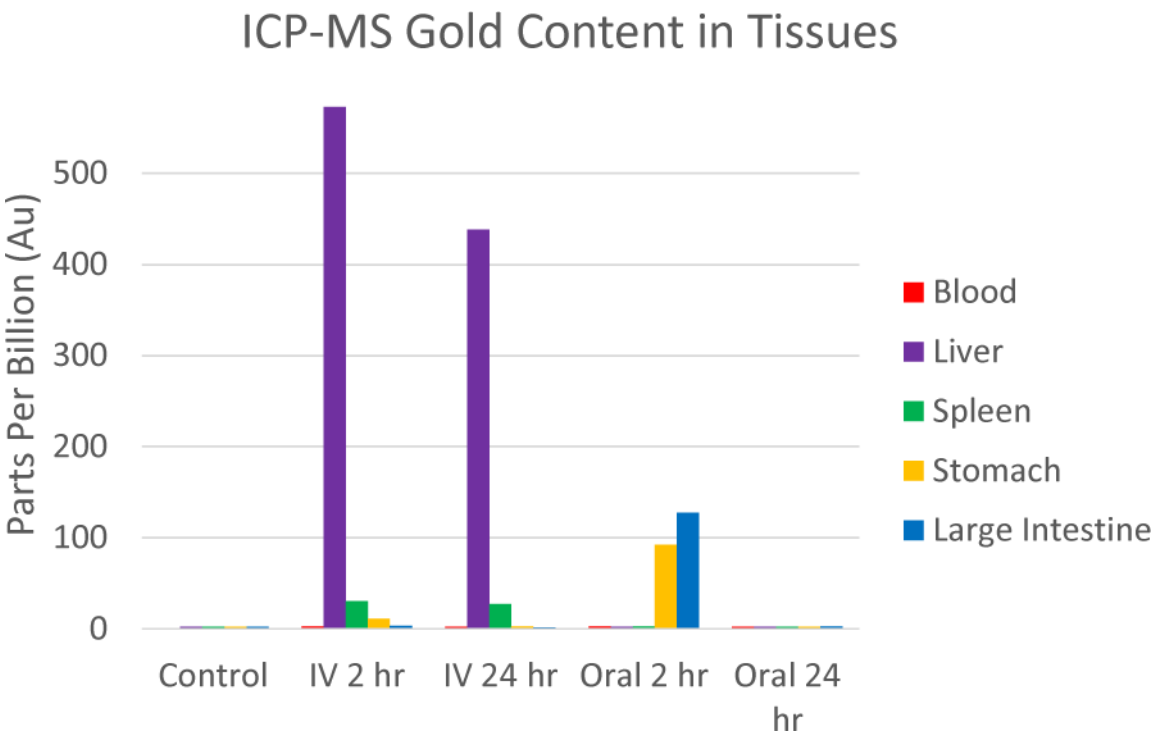

Figure 5.

ICP-MS of gold within tissues of mice injected orally vs intravenously. Notice the consistent levels of gold found within the liver and spleen of the IV injected mice indicating nanoparticle accumulation. Gold was confined to the stomach and large intestine of the orally dosed mice at 2 hours and then completely cleared by 24 hours.

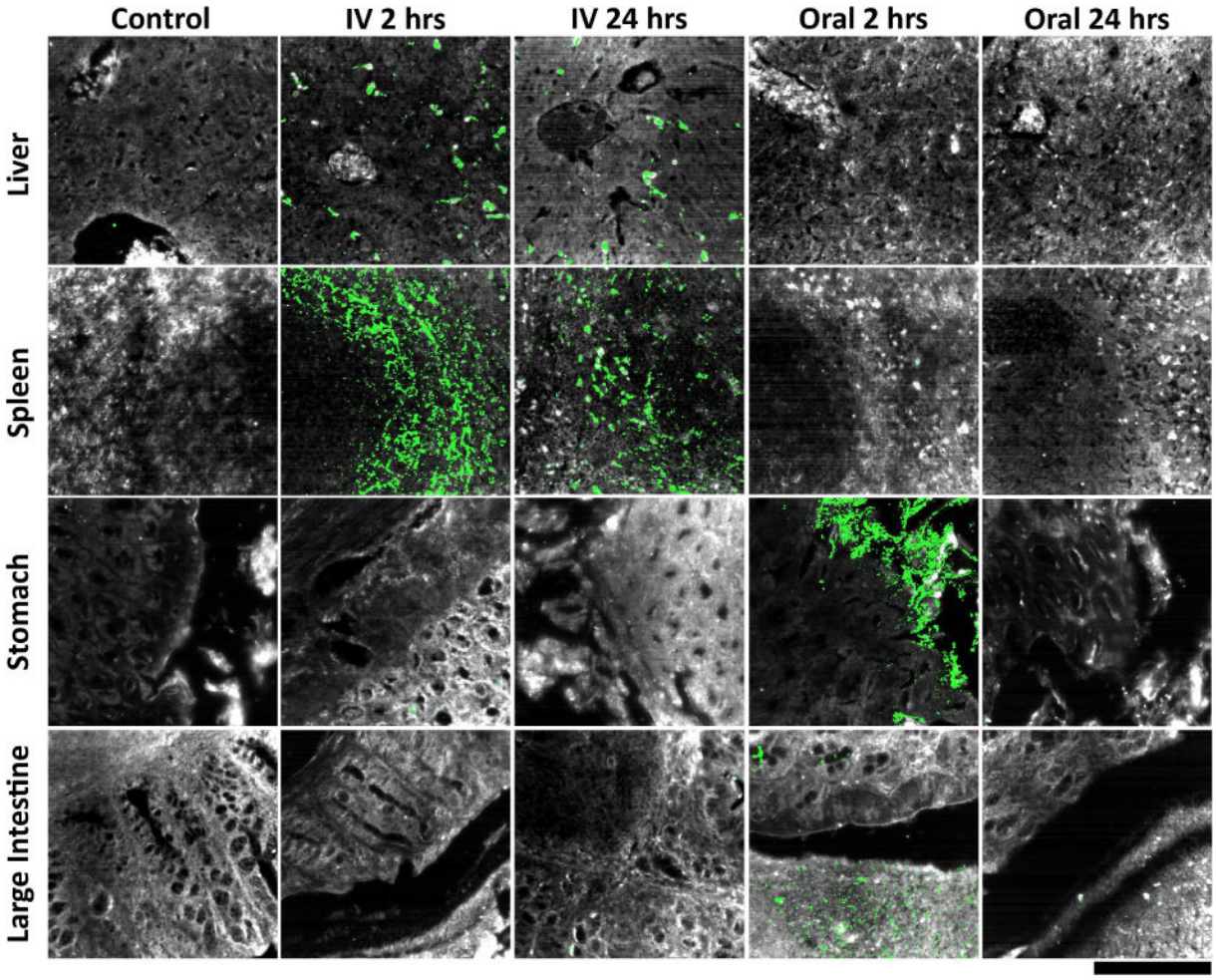

Figure 6.

Hyperspectral detection of particle presence in *ex vivo* tissue sections following intravenous and oral administration. As expected, little to no particle signal was observed in liver, spleen, stomach, and large intestine tissues collected from control mice (far left column). For mice intravenously injected with particles, particle uptake was localized in liver and spleen tissue, while no particle accumulation was apparent within stomach and large intestine tissue 2 hours post-injection (mid-left column). Similar results were observed at 24 hours post-injection, indicating prolonged residence of particles in major clearance organs after intravenous delivery (middle column). By contrast, liver and spleen tissues from mice that received oral particle administration exhibited no particle presence at 2 hours, while stomach and large intestine sections displayed significant particle accumulation (mid-right column). At 24 hours post-oral delivery, particles were not discernible in any of the four tissues analyzed, indicating no translocation to systemic clearance organs as well as virtually complete elimination from the gastrointestinal tract (far-right column). For a quantitative representation of the data please refer to Supplementary Figure S9 within the supporting information. Tissue is depicted in grayscale and particles (identified by their unique spectra) are shown in green for all images presented. Note that these images do not visually convey signal intensity—please refer to Figure S9 for quantitative analysis that does take signal

intensity into account. The scale bar at the bottom right represents 100 μm and applies to all images.

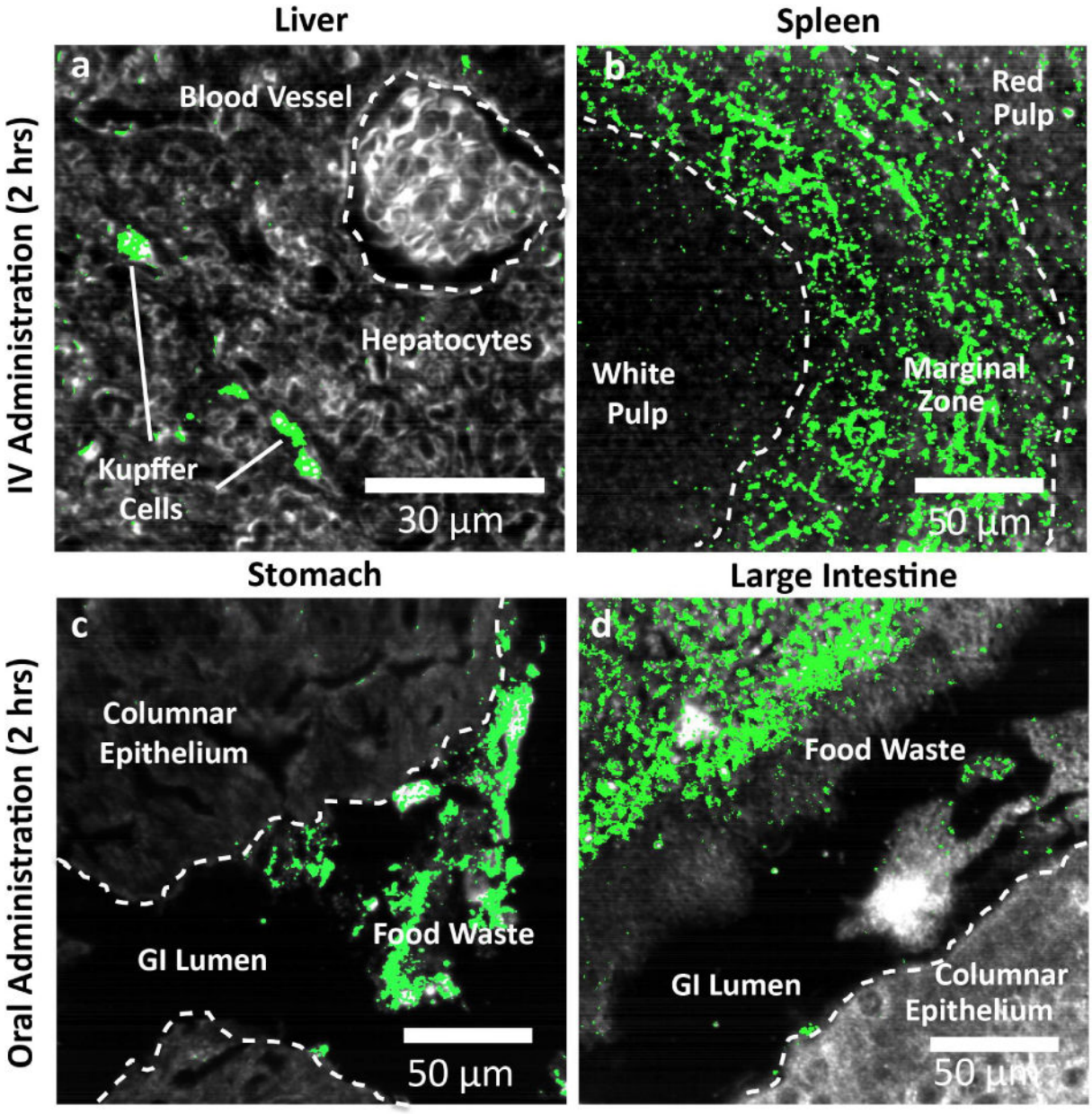

Figure 7.

Histological detail of particle uptake at 2 hours. **a**, IV administered particles accumulate within Kupffer cells in the liver and are mostly absent from other hepatic cell types and blood vessels. **b**, In the spleen, IV administered particles localize mostly within the marginal zone between white pulp follicles and red pulp. While some uptake is observed in the red pulp, virtually no particles are found within the white pulp. **c**, Orally administered particles were observed within the lumen of stomach, however virtually no particles were found within the stomach tissue itself (columnar epithelium). **d**, As in stomach tissue, particles were found exclusively within the waste contents of the gastrointestinal lumen rather than in

the tissue proper. Along with results from 24 hours, these results indicate virtually complete elimination of particles delivered via oral administration.

Table 1

Labeling efficiency and specific activity of varying radiolabeling techniques.

Radiolabeling Scenario	Labeling Efficiency	Specific Activity	Specific Activity
	Percent (%)	mCi/pmol	MBq/pmol
MES pH 5.5 Room Temperature	87.12	14.38	532
MES pH 5.5 60 degrees Celsius	70.31	11.25	416
HEPES pH 8.8 Room Temperature	94.66	15.50	574
HEPES pH 8.8 60 degrees Celsius	94.70	15.63	578
Nanos with DOTA	48.37	11.13	412
Nanos with DOTA and blocked (n-ethyl maleimide)	67.58	15.38	569